arXiv:1303.2822v1 [cond-mat.str-el] 12 Mar 2013

Renormalization group analysis of multi-Dirac-node materials

Hiroki Isobe[1] and Naoto Nagaosa[1,2]
[1]*Department of Applied Physics, University of Tokyo, Tokyo 113-8656, Japan*
[2]*RIKEN Center for Emergent Matter Science, ASI, RIKEN, Wako, Saitama 351-0198, Japan*
(Dated: March 13, 2013)

We theoretically study Dirac systems with N nodes by using the renormalization group (RG), motivated by quantum critical phenomena of topological phase transition and Weyl semimetals. In such materials, the effective energy dispersion is described by Dirac fermions with N species coupled to the electromagnetic field. The RG equations for the coupling constant α, the speed of light c, and electron v are obtained to reveal that (i) c and v coincide in the low-energy limit with c^2v^N being almost unrenormalized, and (ii) there are two momentum/energy scales characterizing nonrelativistic and relativistic scaling regions. The conditions on the materials to observe these scaling behaviors are determined. As for physical quantities, the dielectric constant, magnetic susceptibility, spectral function, DC conductivity, and mass gap are discussed.

PACS numbers: 73.43.Nq, 64.70.Tg, 71.10.-w

I. INTRODUCTION

Dirac fermions are spin 1/2 particles described by the basic equation of the relativistic quantum mechanics, i.e., the Dirac equation.[1] Since it is based on the special relativity, the Dirac equation is invariant under Lorentz transformation. Dirac fermions are described by four-component spinors, and their components correspond to positive and negative energy and spin degrees of freedom. When the mass of a Dirac fermion is nonzero, the four-component representation is irreducible, but in the massless case, it becomes reducible to be two two-component representations. This two-component fermion is called a Weyl fermion. There exists the chiral symmetry for Weyl fermions, so they can be distinguished by the chirality. Right-handed or left-handed Weyl fermions cannot exist independently, thus the number of Weyl fermion is always even. This is the result of the fermion doubling theorem.[2]

The interaction between Dirac fermions and electromagnetic field is formulated in quantum electrodynamics (QED), and the exchange of photons mediates the interaction between electrons. In QED, the speed of electron v and light c has the same value, and QED is the Lorentz-invariant theory.

The electronic states in solids are described by the Bloch wave functions, and according to the band theory, the equation equivalent to the Dirac equation may appear. One such example is graphene, a two-dimensional carbon sheet forming hexagonal lattice.[3] The effective theory is described by the 2×2 Dirac Hamiltonian, and Dirac spectra appear at K and K' points in the Brillouin zone. Another example is bismuth, which exhibits a four-component massive Dirac fermion caused by spin-orbit interaction.[4] Topological insulators with inversion symmetry also have Dirac spectrum on the surface.[5,6] Although the bulk is insulating and gapped in topological insulators, the gap closes at the quantum phase transition between topological and trivial insulators. The effective theory at the critical point is described by the 4×4 Dirac Hamiltonian, and the sign change of mass m corresponds to the phase transition. This story is experimentally confirmed in $\mathrm{BiTl(S_{1-x}Se_x)_2}$ by changing the concentration x.[7,8] Another example is pyrochlore iridates, which are predicted to be Weyl semimetals, where Weyl nodes are located on the Fermi surface. Band calculations indicate that there are 24 (or 8) Weyl nodes exist in pyrochlore iridates.[9,10]

When the Dirac point is located on the Fermi level, the electron-electron interaction is not screened, and remains a long-range force. Thus, the effective model for Dirac fermion in solids has nearly equivalent form to QED. The renormalization group (RG) is used to deal with divergent integrals appearing in the perturbative treatment of the interaction. Here we should note one important difference from QED. In the band theory, the group velocity of electron v is expressed by the derivative of the energy dispersion in terms of the crystal momentum, but this v is far smaller than the speed of light in solids c. Therefore, the Lorentz invariance is terribly broken in this model. The smallness of the factor v/c naturally leads to the choice of Coulomb gauge, where the scalar potential gives the instantaneous Coulomb interaction while the transverse part of the vector potential is often neglected.

The effects of electron-electron interaction on the Dirac electrons are extensively studied.[11–14] The RG analysis of Dirac electrons considering spontaneous Coulomb interaction in two- and three-dimensions[11–13] reveals the logarithmic divergence of v, while the coupling constant α is marginally irrelevant. c is not renormalized, and stays constant. The divergence of v makes the factor v/c larger, and the contribution from the vector potential cannot be ignored. When the contribution from the vector potential is considered for two-dimensional (2D) system, v saturates to c while c remains unchanged, and Lorentz invariance is recovered in the low-energy limit.[14] For 3D system, our previous study[15] reveals the renormalization of c in addition to v, and the recovery of Lorentz invariance in the low-energy limit.

In this paper, we extend the analysis in three dimensions to multi-node Dirac and Weyl systems. The quantum critical phenomenon of topological phase transition and Weyl semimetals are considered as physical realizations of such systems. The transverse current-current interaction due to the vector potential is considered as well as the instantaneous Coulomb interaction. We also corrected some mistakes found in the previous study.[15]

II. MODEL

We start with the following Lagrangian:

$$\mathcal{L} = \bar{\psi}_a(\gamma^0 p_0 - v\boldsymbol{\gamma}\cdot\boldsymbol{p} - m)\psi_a + \frac{1}{2}(\varepsilon\boldsymbol{E}^2 - \frac{1}{\mu}\boldsymbol{B}^2) - e\bar{\psi}_a l^\mu_\nu \gamma^\nu \psi_a A_\mu, \tag{1}$$

where ψ_a is a four-component Dirac spinor with a being the N flavor index, and the matrix

$$l^\mu_\nu = \begin{pmatrix} 1 & & & \\ & v/c & & \\ & & v/c & \\ & & & v/c \end{pmatrix} \tag{2}$$

is defined to describe an electromagnetic interaction in a system without Lorentz invariance. We use a $(+---)$ metric. To separate the temporal and spatial components, we introduce a spatial index $\alpha = 1,2,3$ and $\gamma^\alpha p_\alpha = -\boldsymbol{\gamma}\cdot\boldsymbol{p}$. For the moment, we consider a massless case, i.e., $m = 0$, which corresponds to a quantum critical point of topological insulators and Weyl semimetals. The renormalization of the mass m will be discussed later.

We have dropped the θ term, i.e., $\theta\boldsymbol{E}\cdot\boldsymbol{B}$ $(\theta = \pm\pi)$ in the action, which should be present in the topological insulator phase. This term, however, can be transformed into the surface term, and the sign of θ is determined by the time-reversal symmetry breaking on the surface.[6] The topological magneto-electric effect is derived from this term, but this is beyond the scope of this present analysis, where only the bulk properties are discussed.

Actually the RG analysis does not modify the θ term. It is natural since topological terms have discrete integer values, and we confirmed this fact from the following two methods: the perturbative calculation and the background field theory. In any case, the topological θ term does not alter the bulk properties.

If we consider massless Weyl nodes, the Lagrangian has the chiral symmetry, and the four-component Dirac spinor can be separated into the two-component Weyl spinors with opposite chiralities. Thus, the number of Weyl nodes N_{W} are twice as large as that of Dirac nodes N, i.e., $N_{\mathrm{W}} = 2N$. In the following analysis, we treat the model in the four-component notation. If necessary, we can use the projection operator $(1\pm\gamma^5)/2$ to separate the Dirac fermion into two Weyl fermions with opposite chiralities.

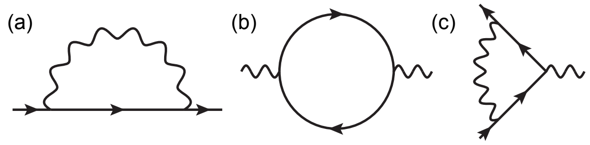

FIG. 1. Feynman diagrams considered here: (a) self-energy, (b) polarization, (c) vertex.

The speed of light in material c and in vacuum $c_{\mathrm{vacuum}} = 3\times 10^8\,\mathrm{m/s}$ are related through the permittivity ε and the permeability μ by $c^2 = c^2_{\mathrm{vacuum}}/(\varepsilon\mu)$. The electric field and magnetic field are represented in terms of the photon field A_μ as

$$\boldsymbol{E} = -\frac{1}{c}\frac{\partial\boldsymbol{A}}{\partial t} - \boldsymbol{\nabla}A_0, \quad \boldsymbol{B} = \frac{1}{c}\boldsymbol{\nabla}\times\boldsymbol{A}. \tag{3}$$

The electron propagator $G_0(p)$, the photon propagator $D^{\mu\nu}_0(p)$, and the vertex Γ^μ_0 are given by

$$G_0(p) = \frac{i}{\gamma^0 p_0 + v\gamma^\alpha p_\alpha + i0}, \tag{4}$$

$$D^{\mu\nu}_0(q) = \frac{-ic^2 g^{\mu\nu}}{\varepsilon(q_0^2 - c^2 q_\alpha^2) + i0}, \tag{5}$$

$$\Gamma^\mu_0 = -iel^\mu_\nu\gamma^\nu = \left(-ie\gamma^0, -ie\frac{v}{c}\gamma^\alpha\right). \tag{6}$$

Here we employ the Feynman gauge because physical quantities are independent of gauge choice.

III. RENORMALIZATION GROUP ANALYSIS

A. Perturbative calculation

Calculations are performed by using dimensional regularization not to violate the gauge invariance of the theory. We set the space-time dimension $d = 4-\epsilon$ to regularize divergences. The self-energy $\Sigma(p)$, polarization $\Pi^{\mu\nu}_2(q)$, and the vertex correction $\delta\Gamma^\mu(p',p)$ are calculated to one-loop order (Fig. 1).

First, we consider the one-loop self-energy contribution [Fig. 1(a)]. According to the Feynman rule, this diagram is calculated by

$$-i\Sigma_2(p) = (-ie)^2\int\frac{d^dk}{(2\pi)^d} l^\mu_\nu\gamma^\nu \frac{i(\gamma^0 k_0 - v\boldsymbol{\gamma}\cdot\boldsymbol{k})}{k_0^2 - v^2\boldsymbol{k}^2} \times l^\rho_\mu\gamma_\rho\frac{-ic^2}{\varepsilon[(p_0-k_0)^2 - c^2(\boldsymbol{p}-\boldsymbol{k})^2]}.$$

After performing the momentum integrals in $(4-\epsilon)$D space, we obtain the one-loop self-energy

$$\Sigma_2(p) = \frac{g^2}{\pi\epsilon}\frac{c}{(c+v)^2}\left[1 - 3\left(\frac{v}{c}\right)^2\right]\gamma^0 p_0 + \frac{g^2}{3\pi\epsilon}\frac{(2c+v)c}{(c+v)^2 v}\left[1 + \left(\frac{v}{c}\right)^2\right]v\boldsymbol{\gamma}\cdot\boldsymbol{p}. \tag{7}$$

For simplicity, we define the effective charge g as

$$g^2 = \frac{e^2}{4\pi\varepsilon}. \tag{8}$$

Next we consider the polarization [Fig. 1(b)], which is given by

$$\begin{aligned} &i\Pi_2^{\mu\nu}(q) \\ &= (-1)N(-ie)^2 \int \frac{d^dk}{(2\pi)^2} \mathrm{tr}\left[l^\mu_\rho \gamma^\rho \frac{i(\gamma^0 k_0 - v\boldsymbol{\gamma}\cdot\boldsymbol{k})}{k_0^2 - v^2\boldsymbol{k}^2} \right. \\ &\quad \left. \times\, l^\nu_\sigma \gamma^\sigma \frac{i(\gamma^0(k_0+q_0) - v\boldsymbol{\gamma}\cdot(\boldsymbol{k}+\boldsymbol{q}))}{(k_0+q_0)^2 - v^2(\boldsymbol{k}+\boldsymbol{q})^2} \right]. \end{aligned}$$

The factor (-1) on the right-hand side comes from the fermion loop. Actually, the polarization is almost the same as that in QED, except the existence of the coefficient $(v/c)^{2-\delta_{\mu0}-\delta_{\nu0}}$. Evaluating the trace over the γ matrices and integrating over momentum space gives

$$\Pi_2^{\mu\nu}(q) = (q^2 g^{\mu\nu} - q^\mu q^\nu)\left(\frac{v}{c}\right)^{2-\delta_{\mu0}-\delta_{\nu0}} \frac{1}{v^3} N\Pi_2(q), \tag{9}$$

where

$$\Pi_2(q) = -\frac{e^2}{6\pi^2\epsilon} + O(\epsilon^0),$$

and $q^\mu = (q^0, vq^\alpha)$ is an electron four-vector.

The remaining diagram we should evaluate is the vertex function [Fig. 1(c)]:

$$\begin{aligned} &\delta\Gamma^\mu(p', p) \\ &= \int \frac{d^dk}{(2\pi)^d} \frac{-ic^2}{\varepsilon[(k_0-p_0)^2 - c^2(\boldsymbol{k}-\boldsymbol{p})^2]} (-iel^\nu_\rho \gamma^\rho) \\ &\quad \times \frac{i(\gamma^0 k'_0 - v\boldsymbol{\gamma}\cdot\boldsymbol{k'})}{k'^2_0 - v^2\boldsymbol{k'}^2} l^\mu_\sigma \gamma^\sigma \frac{i(\gamma^0 k_0 - v\boldsymbol{\gamma}\cdot\boldsymbol{k})}{k_0^2 - v^2\boldsymbol{k}^2} (-iel^\tau_\nu \gamma_\tau), \end{aligned}$$

where $k' = k + p' - p$. The vertex function for the temporal and spatial components are calculated separately, and we obtain

$$\delta\Gamma^0(0,0) = -\frac{g^2}{\pi\epsilon}\frac{c}{(c+v)^2}\left[1 - 3\left(\frac{v}{c}\right)^2\right]\gamma^0, \tag{10a}$$

$$\delta\Gamma^\alpha(0,0) = \frac{g^2}{3\pi\epsilon}\frac{(2c+v)c}{(c+v)^2 v}\left[1 + \left(\frac{v}{c}\right)^2\right]\frac{v}{c}\gamma^\alpha. \tag{10b}$$

B. Renormalization

The diverging quantities appearing through the calculation of the one-loop diagrams are absorbed by adding counterterms and rescaling some quantities. We can write the renormalized Lagrangian $\mathcal{L}_{\mathrm{ren}}$ in the form

$$\mathcal{L}_{\mathrm{ren}} = \mathcal{L}_0 + \mathcal{L}_{\mathrm{c.t.}}, \tag{11}$$

where $\mathcal{L}_0$ is the original Lagrangian and $\mathcal{L}_{\mathrm{c.t.}}$ is the counter term Lagrangian. The counterterms are defined to make the theory finite at the renormalization scale κ_0. In our case, κ_0 corresponds to the cutoff momentum scale.

By defining some new fields and parameters, the renormalized Lagrangian is

$$\begin{aligned} \mathcal{L}_{\mathrm{ren}} =& \bar\psi(Z_{2\mathrm{t}}\gamma^0 p_0 + Z_{2\mathrm{s}} v\gamma^\alpha p_\alpha)\psi \\ &+ \frac{1}{2}(Z_{3\mathrm{e}}\varepsilon\boldsymbol{E}^2 - Z_{3\mathrm{m}}\frac{1}{\mu}\boldsymbol{B}^2) \\ &- Z_{1\mathrm{t}} e\bar\psi\gamma^0\psi A_0 - Z_{1\mathrm{s}} e\frac{v}{c}\bar\psi\gamma^\alpha\psi A_\alpha \\ =& \bar\psi_{\mathrm{B}}(\gamma^0 p_0 + v_{\mathrm{B}}\gamma^\alpha p_\alpha)\psi_{\mathrm{B}} + \frac{1}{2}(\varepsilon_{\mathrm{B}}\boldsymbol{E}_{\mathrm{B}}^2 - \frac{1}{\mu_{\mathrm{B}}}\boldsymbol{B}_{\mathrm{B}}^2) \\ &- e_{\mathrm{B}}\bar\psi_{\mathrm{B}}\gamma^0\psi_{\mathrm{B}}(A_0)_{\mathrm{B}} - e_{\mathrm{B}}\frac{v_{\mathrm{B}}}{c_{\mathrm{B}}}\bar\psi_{\mathrm{B}}\gamma^\alpha\psi_{\mathrm{B}}(A_\alpha)_{\mathrm{B}}. \end{aligned} \tag{12}$$

The subscript B denotes the bare value for each quantity. Each of the field strength renormalization Z is determined from the one-loop result [eqs. (7), (9), (10)] to order g^2. At order g^2, only divergent terms are retained and finite terms are ignored, since finite terms have no effect in the RG calculation. The results are

$$Z_{1\mathrm{t}} = 1 + \frac{g^2}{\pi\epsilon}\frac{c}{(c+v)^2}\left[1 - 3\left(\frac{v}{c}\right)^2\right], \tag{13}$$

$$Z_{1\mathrm{s}} = 1 - \frac{g^2}{3\pi\epsilon}\frac{(2c+v)c}{(c+v)^2 v}\left[1 + \left(\frac{v}{c}\right)^2\right], \tag{14}$$

$$Z_{2\mathrm{t}} = 1 + \frac{g^2}{\pi\epsilon}\frac{c}{(c+v)^2}\left[1 - 3\left(\frac{v}{c}\right)^2\right], \tag{15}$$

$$Z_{2\mathrm{s}} = 1 - \frac{g^2}{3\pi\epsilon}\frac{(2c+v)c}{(c+v)^2 v}\left[1 + \left(\frac{v}{c}\right)^2\right], \tag{16}$$

$$Z_{3\mathrm{e}} = 1 - \frac{2Ng^2}{3\pi\epsilon}\frac{1}{v}, \tag{17}$$

$$Z_{3\mathrm{m}} = 1 - \frac{2Ng^2}{3\pi\epsilon}\frac{v}{c^2}. \tag{18}$$

Here we can confirm $Z_{1\mathrm{t}} = Z_{2\mathrm{t}}$ and $Z_{1\mathrm{s}} = Z_{2\mathrm{s}}$. These relations are consequences of the Ward-Takahashi identity. The bare quantities are defined by using the field strength renormalization as

$$\psi_{\mathrm{B}} = Z_{2\mathrm{t}}^{1/2}\psi, \tag{19}$$

$$v_{\mathrm{B}} = \frac{Z_{2\mathrm{s}}}{Z_{2\mathrm{t}}}v, \tag{20}$$

$$\varepsilon_{\mathrm{B}}(A_0)_{\mathrm{B}}^2 = Z_{3\mathrm{e}}\varepsilon A_0^2, \tag{21a}$$

$$\varepsilon_{\mathrm{B}}\left(\frac{(A_\alpha)_{\mathrm{B}}}{c_{\mathrm{B}}}\right)^2 = Z_{3\mathrm{e}}\varepsilon\left(\frac{A_\alpha}{c}\right)^2, \tag{21b}$$

$$\frac{1}{\mu_{\mathrm{B}}}\left(\frac{(A_\alpha)_{\mathrm{B}}}{c_{\mathrm{B}}}\right)^2 = Z_{3\mathrm{m}}\frac{1}{\mu}\left(\frac{A_\alpha}{c}\right)^2, \tag{22}$$

$$c_{\mathrm{B}} = \sqrt{\frac{Z_{3\mathrm{m}}}{Z_{3\mathrm{e}}}}c, \tag{23}$$

$$g_{\mathrm{B}} = \frac{Z_{1\mathrm{t}}}{Z_{2\mathrm{t}}Z_{3\mathrm{e}}^{1/2}}g = \frac{Z_{1\mathrm{s}}}{Z_{2\mathrm{s}}Z_{3\mathrm{e}}^{1/2}}g = Z_{3\mathrm{e}}^{-1/2}g. \tag{24}$$

These bare quantities must be independent of the renormalization scale κ_0. We use this fact to derive RG equations afterward.

C. The Ward-Takahashi identity

We should confirm that the self-energy [eq. (7)] and the vertex correction [eq. (10)] satisfy the Ward-Takahashi identity. Here we consider the model without the Lorentz invariance, i.e. $v \neq c$, we should be careful about the coefficients of the self-energy and the vertex correction.

The Ward-Takahashi identity is

$$-ik_\mu \Gamma^\mu(p+k,p) = G^{-1}(p+k) - G^{-1}(p), \tag{25}$$

where $G(p)$ is an exact fermion propagator

$$G(p) = \frac{i}{\gamma^0 p_0 - v\boldsymbol{\gamma}\cdot\boldsymbol{p} - \Sigma(p)}, \tag{26}$$

and $\Gamma^\mu(p+k,p)$ is an exact vertex. An important point here is that k_μ in the left-hand side of eq. (26) comes from the photon propagator, so k_μ must be interpreted as $k^\mu = (k^0, ck^\alpha)$. This formula holds even in this broken Lorentz invariance case.

From the Ward-Takahashi identity, we can find the relation between Z_1 and Z_2. We separate the electron self-energy into the temporal and spatial parts as

$$\Sigma(p) = \Sigma^{(\mathrm{t})}\gamma^0 p_0 + \Sigma^{(\mathrm{s})} v\gamma^\alpha p_\alpha. \tag{27}$$

Then the Ward-Takahashi identity becomes

$$\begin{aligned} &-ik_0(\Gamma^0_0 + \delta\Gamma^0) - ick_\alpha(\Gamma^\alpha_0 + \delta\Gamma^\alpha) \\ &= -i(1+\Sigma^{(\mathrm{t})})\gamma^0 k_0 - i(1+\Sigma^{(\mathrm{s})})v\gamma^\alpha k_\alpha. \end{aligned} \tag{28}$$

Each quantity in parenthesis corresponds to Z_1 or Z_2, except that the spatial component of the vertex correction includes a factor v/c. Therefore, we obtain

$$Z_{1\mathrm{t}} = Z_{2\mathrm{t}}, \tag{29a}$$

$$Z_{2\mathrm{s}} = Z_{2\mathrm{s}}. \tag{29b}$$

D. Derivation of the renormalization group equations

Before deriving RG equations, it is important to check the dimensions of several quantities. From the dimension of a quantity, we can easily presume the dependence of the quantity on the momentum scale. We denote the physical dimensions of wavenumber [(length)$^{-1}$] and frequency [(time)$^{-1}$] as Λ and Ω, respectively. We can determine the dimension of the Lagrangian, since the action should be dimensionless. Thus,

$$[\mathcal{L}] = [\Lambda^{d-1}\Omega^1]. \tag{30}$$

Then considering the Lagrangian (1), we can obtain other relations as

$$[\psi] = [\Lambda^{(d-1)/2}], \tag{31}$$

$$[\varepsilon E^2] = [\Lambda^{d-1}\Omega^1], \tag{32}$$

$$[eE] = [\Lambda^1\Omega^1], \tag{33}$$

$$[g^2] = [\Lambda^{3-d}\Omega^1] = [(\mathrm{velocity})^1\Lambda^\epsilon]. \tag{34}$$

To explicitly represent the engineering dimension of g^2, we substitute g^2 with $g^2\kappa^\epsilon$ in the original Lagrangian $\mathcal{L}$ and the counterterm Lagrangian $\mathcal{L}_{\mathrm{c.t.}}$. The bare values are momentum-scale invariant, so the bare value g_{B} does not change.

Then, we can derive the RG equations from the fact that bare values are independent of the momentum scale κ. While the physical values v, c, and g are functions of the mometum scale κ, the bare quantities does not depend on κ. Thus, from eqs. (20), (23), and (24), we obtain the RG equations

$$\kappa\frac{dv}{d\kappa} = -\frac{2g^2}{3\pi}\frac{c^2}{(c+v)^2}\left[1 + 2\left(\frac{v}{c}\right) + \left(\frac{v}{c}\right)^2 - 4\left(\frac{v}{c}\right)^3\right], \tag{35}$$

$$\kappa\frac{dc}{d\kappa} = \frac{Ng^2}{3\pi}\frac{c^2-v^2}{cv}, \tag{36}$$

$$\kappa\frac{dg^2}{d\kappa} = \frac{2Ng^4}{3\pi}\frac{1}{v} \tag{37}$$

in the limit $\epsilon \to 0$.

E. Numerical solutions

The RG equations (35), (36), (37) cannot be solved analytically without any approximations, so we first solve them numerically. The numerical solutions for the RG equations are shown in Figs. 2 and 3 for the initial (bare) values of $v_0 = 0.001$ and $\varepsilon_0 = 10$. Here we consider a nonmagnetic material ($\mu_0 = 1$). In this case, $c_0 = 0.32$ and $\alpha_0 = 0.73$, where the dimensionless coupling constant α is defined by

$$\alpha = \frac{g^2}{v} = \frac{e^2}{(4\pi\varepsilon)v}. \tag{38}$$

The result shows some important features. First, we can see that the quantity c^2v^N is almost constant for all momentum scales and remains $c_0^2v_0^N$. This fact helps the approximate but accurate analysis of the scaling functions as described below. Second, the speed of electron v and that of photon c approach to the common value $c_\infty = (c_0^2v_0^N)^{1/(N+2)}$ in the infrared (IR) limit. Third, the coupling constant α becomes small in the IR region, which justifies our perturbative RG analysis. Therefore, quantum critical phenomena of 3D topological insulators and Weyl semimetals are ideal laboratories to study the QED in solids, even though the Lorentz invariance is broken to a large extent in the original (bare) Lagrangian.

F. Analytic solutions

In this section, we investigate the analytic expressions for the RG equations. First, we define $l = \ln(\kappa_0/\kappa)$ and consider the quantity c^2v^N. From the RG equations, the

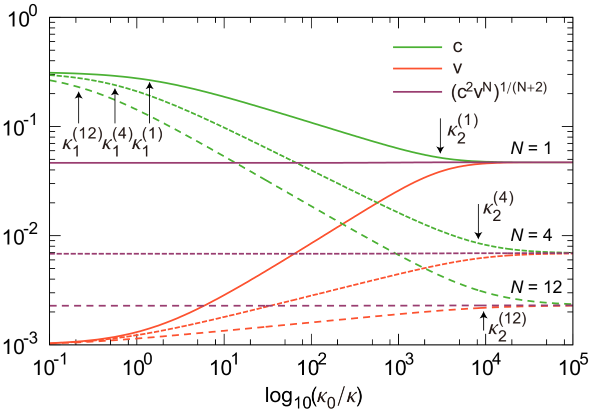

FIG. 2. (Color online) Numerical solutions to the RG equations for v and c. We set the initial values $v_0 = 0.001$ and $\varepsilon_0 = 10$. A nonmagnetic material ($\mu_0 = 1$) is considered, and in this case, $c_0 = 0.32$ and $\alpha_0 = 0.73$. We can observe that the quantities $(c^2v^N)^{1/(N+2)}$ are almost constant for all momentum scale.

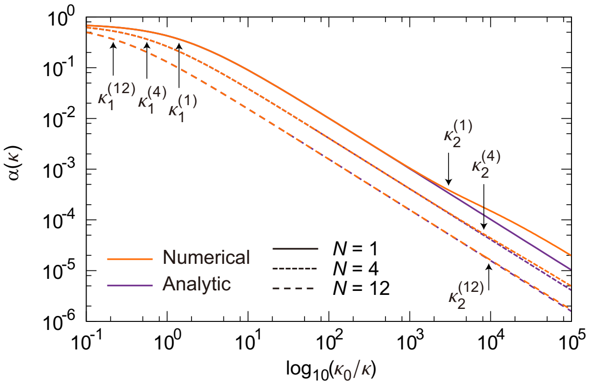

FIG. 3. (Color online) Numerical and analytic solutions to the RG equations for α. The analytic solutions well explain the numerical solutions for $\kappa \gtrsim \kappa_2$. As the number of species N increases, the difference between the analytic and numerical solutions becomes smaller, and the analytic expression is more precise.

scale dependence of the quantity is

$$\begin{aligned}\frac{d(c^2v^N)}{dl} =& 2cv^N\frac{dc}{dl} + Nc^2v^{N-1}\frac{dv}{dl}\\ =& \frac{2Ng^2}{3\pi}c^2v^{N-1}\frac{\beta^2(1-\beta)^2}{(1+\beta)^2},\end{aligned} \tag{39}$$

where $\beta = v/c$. If we define the function $f(\beta)$ as

$$f(\beta) = \frac{\beta^2(1-\beta)^2}{(1+\beta)^2}, \tag{40}$$

and assume $v \le c$, i.e. $0 \le \beta \le 1$, we obtain $0 \le f(\beta) \le 17 - 12\sqrt{2} \simeq 0.03$. The maximum value $g(\beta) \simeq 0.03$ is rarely observed in the scale of Fig. 2, and the right-hand side of eq. (39) is always small for $0 < \beta < 1$. Therefore, the approximation

$$c^2v^N = c_0^2v_0^N \tag{41}$$

is satisfied for the entire energy scale.

The second approximation is

$$\frac{c}{c_0} = \frac{g}{g_0}. \tag{42}$$

It holds until c reaches the vicinity of the asymptotic value c_∞. Actually, this approximation has a physical interpretation. Since $c = 1/\sqrt{\varepsilon\mu}$ and $g = e/\sqrt{4\pi\varepsilon}$, the equality means the permeability μ stays constant.

Using eqs. (41), (42), we can analytically solve the RG equations (35), (36), and (37), and obtain

$$g^2(l) = g_0^2\left(1 + \frac{2N+2}{3\pi}\alpha_0 l\right)^{-N/(N+1)}. \tag{43}$$

The other solutions follow by using the analytic expression of $g^2(l)$ as

$$v(l) = v_0\left(1 + \frac{2N+2}{3\pi}\alpha_0 l\right)^{1/(N+1)}, \tag{44}$$

$$c(l) = c_0\left(1 + \frac{2N+2}{3\pi}\alpha_0 l\right)^{-N/(2N+2)}, \tag{45}$$

$$\alpha(l) = \alpha_0\left(1 + \frac{2N+2}{3\pi}\alpha_0 l\right)^{-1}. \tag{46}$$

These analytic expressions are valid for $\kappa \gtrsim \kappa_2$.

From the analytical solutions, we can identify the two momentum scales, κ_1 and κ_2, as

$$\kappa_1^{(N)} = \exp\left[-\frac{3\pi}{(2N+2)\alpha_0}\right], \tag{47a}$$

$$\kappa_2^{(N)} = \exp\left[-\frac{3\pi}{(2N+2)\alpha_0}\left[\left(\frac{c_0}{v_0}\right)^{(2N+2)/(N+2)} - 1\right]\right]. \tag{47b}$$

κ_1 is determined by $\alpha(\kappa_1) = \alpha_0/2$ and κ_2 is the point where the analytically-derived function $c(\kappa)$ coincides the asymptotic value c_∞. Assuming $v_0/c_0 \ll 1$, $\kappa_2 \ll \kappa_1 < \kappa_0$ is satisfied. These two momenta separate the three regions: (i) perturbative region $\kappa_1 \lesssim \kappa \lesssim \kappa_0$, the renormalization effect is small and perturbative; (ii) nonrelativistic scaling region $\kappa_2 \lesssim \kappa \lesssim \kappa_1$, the renormalization effect is large, while $c(\kappa) \gg v(\kappa)$ still holds; and (iii) relativistic scaling region $\kappa \lesssim \kappa_2$, $c(\kappa) \simeq v(\kappa)$ and the Lorentz invariance is recovered.

IV. DENSITY OF STATES

The DOS is an important quantity to determine the physical property of a material. From the RG analysis, the electron velocity $v(k)$ is not a constant, and the energy $E(k) = v(k)k$ is no longer linear in the momentum

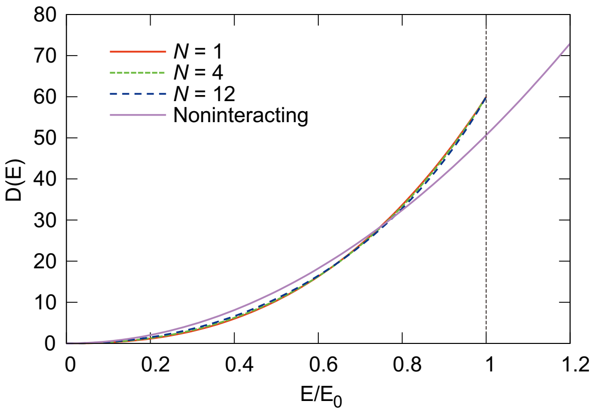

FIG. 4. (Color online) Density of states modified by the RG analysis. The DOS in the low-energy region is suppressed compared to the noninteracting one, due to the electron correlation effect. To compensate the suppression, the DOS increases around $E/E_0 \gtrsim 0.8$. The effect of RG appears only below the cutoff energy E_0.

k below the cutoff. In general, the DOS of a system with energy $E(k)$ is determined as

$$D(E) = \int \frac{d^3k}{(2\pi)^3}\delta(E - E(k)) = \frac{1}{2\pi^2}\frac{k^2(E)}{E'(k(E))}, \quad (48)$$

where E' stands for dE/dk. The DOS is a function of energy, so all quantities should be expressed in terms of energy E.

The DOS for 3D noninteracting Dirac fermions is

$$D_0(E) = \frac{E^2}{2\pi^2 v_0^3}. \quad (49)$$

The RG effect on the DOS is calculated numerically, and is compared with the noninteracting case in Fig. 4. Since $v(k)$ gets faster as the momentum scale goes to the infrared region, the DOS is suppressed in the low-energy region. On the other hand, the DOS is increased for $0.8 \lesssim E/E_0 < 1$, where $E_0 = v_0\kappa_0$ is the energy cutoff. This increase compensate the suppression of the DOS in the low-energy region.

V. ELECTROMAGNETIC PROPERTIES

Let us discuss the permittivity $\varepsilon(\kappa)$ and the permeability $\mu(\kappa) = 1 + 4\pi\chi$ (χ: magnetic susceptibility). The numerical solutions obtained from eq. (37) and $\mu = 1/(\varepsilon c^2)$ are shown in Fig. 5. We consider that the scale dependence of g^2 emerges only from ε, and that the bare electric charge e stays constant. For $\kappa \gtrsim \kappa_2$, the analytic solution to ε is easily obtained from eq. (43) as

$$\varepsilon(l) = \varepsilon_0 \left(1 + \frac{2N+2}{3\pi}\alpha_0 l\right)^{N/(N+1)}. \quad (50)$$

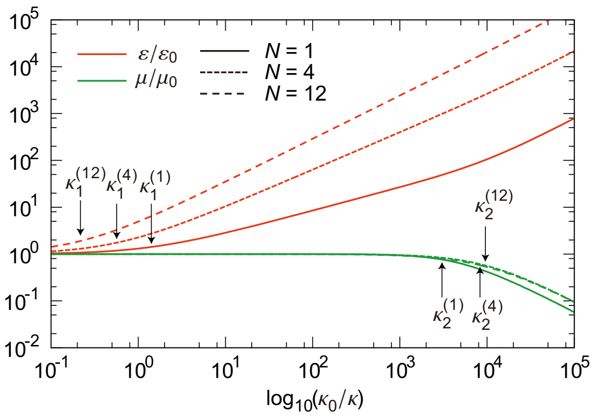

FIG. 5. (Color online) Numerical solutions to the RG equations for the permittivity ε and the permeability μ. The characteristic momentum scales are different for ε and μ.

The momentum scale κ can be regarded as the temperature T by $T \simeq v(\kappa)\kappa$. As noted above, the velocity $v(\kappa)$ is the function of the momentum scale, hence the energy dispersion $E(k) = v(k)k$ is a nonlinear function of k. From the definition of κ_1 and κ_2, $v(\kappa_1) \simeq v_0$ and $v(\kappa_2) \simeq c_\infty$, and the corresponding temperatures are estimated as $T_1 = T(\kappa_1) \simeq v_0\kappa_1$ and $T_2 = T(\kappa_2) \simeq c_\infty\kappa_2$. In Fig. 5, it can be seen that the permittivity $\varepsilon(\kappa)$ grows logarithmically below T_1 while the permeability $\mu(\kappa)$ decreases below T_2. The orbital magnetic susceptibility χ without the electron-electron interaction logarithmically diverges as a function of T, but in our analysis, the logarithmic divergence is canceled due to the renormalization of v. These contrasting behaviors of ε and μ facilitate the identification of T_1 and T_2 experimentally. In the zero temperature limit ε diverges while μ goes to zero, i.e., the perfect diamagnetism $\chi = -1/(4\pi)$ is accomplished.

VI. SPECTRAL FUNCTION

To derive the spectral function as the imaginary part of the Green's function, we should be careful on the choice of the gauge, because the Green's function itself depends on the gauge. We adopt the "physical gauge," i.e., Coulomb gauge. In Coulomb gauge, the photon propagator $D_{\mathrm{C}}^{\mu\nu}(k)$ is given by[16]

$$D_{\mathrm{C}}^{\mu\nu}(k) = \frac{c^2}{\varepsilon}\begin{pmatrix} \dfrac{1}{\boldsymbol{k}^2} & 0 \\ 0 & -\dfrac{g^{\alpha\beta}}{k^2} - \dfrac{1}{k^2}\dfrac{k^\alpha k^\beta}{\boldsymbol{k}^2} \end{pmatrix}. \quad (51)$$

We need to calculate the one-loop self-energy [Fig. 1(a)] by using the photon propagator in Coulomb gauge. The electron propagator is the same as before. After some calculation, we obtain the one-loop self-energy in Coulomb gauge $\Sigma_2^{(\mathrm{C})}(p)$ as

$$\begin{aligned}\Sigma_2^{(\mathrm{C})}(p) =& -\frac{2g^2}{\pi}\frac{v^2}{c(c+v)^2}\left(\frac{1}{\epsilon}-\frac{1}{2}\ln\frac{e^\gamma}{4\pi}\right)\gamma^0 p_0\\ &+\frac{2g^2}{3\pi}\frac{c^2}{v(c+v)^2}\left[1+2\left(\frac{v}{c}\right)+\left(\frac{v}{c}\right)^2-\left(\frac{v}{c}\right)^3\right]\\ &\times\left(\frac{1}{\epsilon}-\frac{1}{2}\ln\frac{e^\gamma}{4\pi}\right)v\boldsymbol{\gamma}\cdot\boldsymbol{p}, \end{aligned}\tag{52}$$

where $\gamma \approx 0.57721$ is the Euler-Mascheroni constant. For a later use, we show the result to order $O(\epsilon^0)$. The self-energy in Coulomb gauge [eq. (52)] is different from the self-energy in Feynman gauge [eq. (7)], comparing the $O(\epsilon)$ contributions.

The field strength renormalization $Z_{2\mathrm{t}}^{(\mathrm{C})}$ and $Z_{2\mathrm{s}}^{(\mathrm{C})}$ in Coulomb gauge are

$$Z_{2\mathrm{t}}^{(\mathrm{C})} = 1-\frac{2g^2}{\pi\epsilon}\frac{v^2}{c(c+v)^2},\tag{53}$$

$$Z_{2\mathrm{s}}^{(\mathrm{C})} = 1-\frac{2g^2}{3\pi\epsilon}\frac{c^2}{v(c+v)^2}\left[1+2\left(\frac{v}{c}\right)+\left(\frac{v}{c}\right)^2-\left(\frac{v}{c}\right)^3\right].\tag{54}$$

This difference alters the Green's function and also the spectral function, while the physical quantities, e.g. the electron velocity v, remain the same.[17] For the spectral function of electrons, the function $\gamma_2(\kappa)$ in Coulomb gauge is required, which is given by

$$\gamma_2^{(\mathrm{C})}(v,c,\alpha;\kappa) = \frac{1}{2}\kappa\frac{d\ln Z_{2\mathrm{t}}}{d\kappa} = \frac{g^2}{\pi}\frac{v^2}{c(c+v)^2}.\tag{55}$$

In principle, ARPES can measure the energy dispersion $E(k) = v(\kappa)|\boldsymbol{k}|$, which shows crossovers at κ_1 and κ_2. From the Callan-Symanzik equation, the electron Green's function in Coulomb gauge $G^{(\mathrm{C})}(\boldsymbol{k},\omega)$ is

$$G^{(\mathrm{C})}(\boldsymbol{k},\omega) = \frac{\mathcal{G}(\alpha(\kappa))}{\omega^2-v^2(\kappa)\boldsymbol{k}^2}\exp\left[2\int_\Lambda^k d\ln\left(\frac{k'}{\Lambda}\right)\gamma_2(\alpha)\right].\tag{56}$$

k in this equation should be considered as a spacelike vector, and $k = \sqrt{v^2\boldsymbol{k}^2-\omega^2}$.

In region (i), $\gamma_2 = 0$, so the Green's function is unchanged. In region (ii), κ dependence of γ_2 is rather complicated to calculate $G(\boldsymbol{k},\omega)$, so we only consider the relativistic scaling region (iii), where v approaches c and the original QED regime is applicable. When we put $c = v = c_\infty$, the RG equation for α becomes

$$\frac{d\alpha}{dl} = -\frac{2N}{3\pi}\alpha^2,\tag{57}$$

and it can be solved analytically to obtain

$$\alpha(l) = \frac{3\pi}{2N}\frac{1}{l}.\tag{58}$$

Surprisingly, the coupling constant $\alpha(l)$ in region (iii) is independent of its bare value α_0. Then $\gamma_2^{(\mathrm{C})}(k)$ is expressed as

$$\gamma_2^{(\mathrm{C})}(k) = \frac{\alpha(k)}{4\pi} = \frac{3}{8N}\left[\ln\left(\frac{\Lambda}{k}\right)\right]^{-1}.\tag{59}$$

The perturbative correction $\mathcal{G}$ is obtained from the $O(\epsilon)$ contribution of $\Sigma_2^{(\mathrm{C})}(p)$ [eq. (52)], since the divergent part, proportional to $1/\epsilon$ is eliminated by the counterterms. Therefore the perturbative correction $\mathcal{G}$ is

$$\mathcal{G}(\alpha(k)) = 1+\frac{\alpha(k)}{4\pi}\ln\left(\frac{e^\gamma}{4\pi}\right)+O(\alpha^2).\tag{60}$$

Finally, we obtain the electron Green's function

$$G(\boldsymbol{k},\omega) = \frac{\mathcal{G}(\alpha(k))}{\omega^2-c_\infty^2\boldsymbol{k}^2}\left[\frac{1}{2}\ln\left(\frac{\Lambda^2}{c_\infty^2\boldsymbol{k}^2-\omega^2}\right)\right]^{-3/(4N)}.\tag{61}$$

By substituting ω with $\omega+i0$, the imaginary part of the Green's function $-\mathrm{Im}G(\boldsymbol{k},\omega)$ gives the electron spectral function. The electron spectral function has finite value for $|\omega| \geq c_\infty|\boldsymbol{k}|$, otherwise $-\mathrm{Im}G(\boldsymbol{k},\omega) = 0$. The perturbative correction for $\mathcal{G}$ gives very small contribution, so we put $\mathcal{G} = 1$ in the following analysis. Then, the spectral function in region (iii) has the approximate form

$$\begin{aligned}&-\mathrm{Im}G(\boldsymbol{k},\omega)\\ \sim\, & a\delta(\omega^2-c_\infty^2\boldsymbol{k}^2)\\ &+\frac{1}{\omega^2-c_\infty^2\boldsymbol{k}^2}\frac{3\pi}{8N}\left[\frac{1}{2}\ln\left|\frac{\Lambda^2}{c_\infty^2\boldsymbol{k}^2-\omega^2}\right|\right]^{-1-3/(4N)}\\ &\times\theta(\omega^2-c_\infty^2\boldsymbol{k}^2),\end{aligned}\tag{62}$$

where the residue a is a constant determined from the sum rule. The δ function peak with finite a means that the system remains a Fermi liquid in sharp contrast to the (2+1)D case,[14] while the continuum state for $|\omega| > c_\infty k$ comes from the interaction.

VII. ELECTRIC CONDUCTIVITY

In this section, we calculate the electric conductivity from the quantum Boltzmann equation with the leading log approximation. Calculations are performed by following previous studies,[13,18,19] and the detailed description is shown in Appendix. We present only the solution here, which is valid for $\omega \ll T$:

$$\begin{aligned}&\sigma^{(N)}(\omega,T)\\ =&N_{\mathrm{W}}\frac{e^2}{h^2}\left(\frac{k_{\mathrm{B}}T}{\hbar v}\right)\frac{243[\zeta(3)]^2}{4\pi^4}\\ &\times\left[N_{\mathrm{W}}(\alpha^2\ln\alpha^{-1})F\left(\frac{v}{c}\right)-\frac{21\pi}{20}i\beta\omega\right]^{-1},\end{aligned}\tag{63}$$

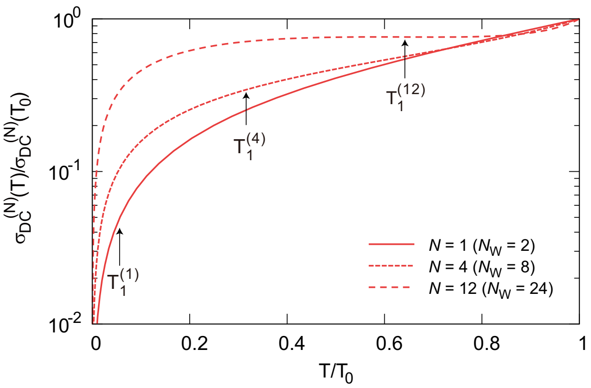

FIG. 6. (Color online) DC conductivity $\sigma_{\mathrm{DC}}^{(N)}(T)$.

where the function $F(x)$ is

$$F(x) = 1 + \frac{1}{4}\left[3 - x^2 - \frac{(1-x^2)(3+x^2)}{x}\tanh^{-1} x\right]. \tag{64}$$

We recovered k_{B} and $\hbar$ in the last line of eq. (63). The function $F(v/c)$ can be regarded as the relativistic correction, and it cannot be obtained from the nonrelativistic analysis.[13] In the nonrelativistic limit ($v/c \to 0$), we have $F(v/c) = 1$, and it monotonically increases to $F(v/c) = 3/2$ ($v/c \to 1$). Especially, the DC conductivity is

$$\sigma_{\mathrm{DC}}^{(N)}(T) = \frac{e^2}{h}\frac{k_{\mathrm{B}}T}{\hbar v}\frac{0.90}{\alpha^2 \ln \alpha^{-1} F(v/c)}, \tag{65}$$

and shown in Fig. 6.

VIII. ENERGY GAP

Up to now, we have focused on the critical point ($m = 0$), but the mass m is a relevant parameter. Experimentally, the bare mass m_0 can be controlled by the concentration x or by pressure P.[7,8] The RG equation for mass $m(\kappa)$ is

$$\kappa\frac{dm}{d\kappa} = -\frac{3\alpha}{2\pi}m. \tag{66}$$

Then, the mass at momentum scale κ is

$$m(\kappa) = m(\Lambda)\left[1 + \frac{2N+2}{3\pi}\alpha_0 \ln\left(\frac{\Lambda}{\kappa}\right)\right]^{9/(4N+4)}. \tag{67}$$

When we neglect the weak singularity with $\ln\ln m_0$, the solution to eq. (67) is given by

$$m = m_0\left[1 + \frac{2N+2}{3\pi}\alpha_0 \ln\left(\frac{\Lambda}{m_0}\right)\right]^{9/(4N+4)}, \tag{68}$$

which describes the critical behavior of the gap as a function of $m_0 \propto (x - x_c)$ or $m_0 \propto (P - P_c)$ with x_c (P_c) being the critical concentration (pressure).

IX. DISCUSSIONS AND SUMMARY

Now we discuss the relevance of the present results to the real systems.

First, for a topological insulator ($N = 1$), the velocity v_0 is estimated at $v_0 \simeq 10^6\,\mathrm{m/s}$ from the ARPES measurement of the energy dispersion,[7] hence $c_{\mathrm{vacuum}}/v_0 \simeq 300$. As the dielectric constant, we take the typical value $\varepsilon_0 \simeq 10^2$ for BiSb alloys.[20] Since $c_0 = c_{\mathrm{vacuum}}/\sqrt{\varepsilon_0}$, $c_0/v_0 \simeq 30$ and $\alpha_0 = (1/137)/(\varepsilon v) \simeq 0.022$ are obtained. These values give the estimates for $\kappa_1 \simeq 10^{-47}\kappa_0$ and $\kappa_2 \ll \kappa_1$.

For the pyrochore iridate $\mathrm{Y_2Ir_2O_7}$ with $N = 12$ ($N_{\mathrm{W}} = 24$), the velocity and the dielectric constant may be estimated as $v_0 \simeq 10^6\,\mathrm{m/s}$ and $\varepsilon_0 \simeq 10$.[13] In this case $c_0/v_0 \simeq 95$ and $\alpha_0 \simeq 0.22$, so we obtain $\kappa_1 \simeq 0.2\kappa_0$, and κ_2 is extremely small. The value $\kappa_1 \simeq 0.2\kappa_0$ would be physically accessible.

To experimentally observe the RG effects, we have to search materials with reasonably large κ_1 and κ_2. A larger coupling constant α_0 is necessary to obtain larger κ_1, and this can be realized if both of the dielectric constant ε_0 and the Fermi velocity v are small. In addition to large α_0, small c_0/v_0 is required to make κ_2 larger. There seem to be two approaches: (a) small c_0 and (b) large v_0. In case (a), a large dielectric constant ε_0 leads to the small coupling constant α_0 (assuming $\mu_0 = 1$), so it cannot be a solution. In case (b), a large v_0 also brings a small α_0. The only way out is the small ratio of c_0/v_0. Unfortunately, it would be difficult to observe the relativistic scaling behavior at the experimentally accessible temperature in the materials at hand.

This estimation gives a justification for the nonrelativistic approximation. Physically accessible κ_1 is easily obtained by choosing appropriate v_0 and ε_0, but it would be difficult to access κ_2 unless $c_0 \approx v_0$. It means that the nonrelativistic approximation in the RG analysis is adequate in ordinary situations. However, if $c_0 \approx v_0$ is accomplished with $\varepsilon_0 \sim 1$ and $\mu_0 \gg 1$, we might reach κ_2, i.e., the relativistic scaling region.

In summary, we have studied the (3+1)D Dirac electrons coupled to electromagnetic field as the model for quantum critical phenomena of the topological phase transition and Weyl semimetals. The RG equations are derived and the two scaling regions are identified, i.e., the perturbative, nonrelativistic and relativistic scaling regions. The Lorentz invariance is recovered in the third case. The physical properties such as the the permittivity, the permeability, the electron spectral function, the conductivity, and the mass gap have been discussed based on the RG equations.

ACKNOWLEDGMENTS

We acknowledge fruitful discussions with S. Nakosai. This work is supported by Grant-in-Aid for Scientific Research (Grant No. 24224009) from the Ministry of Education, Culture, Sports, Science and Technology of Japan, Strategic International Cooperative Program (Joint Research Type) from Japan Science and Technology Agency, and Funding Program for World-Leading Innovative RD on Science and Technology (FIRST Program).

Appendix: Derivation of the electric conductivity

In the appendix, we derive the conductivity of the system with N_{W} Weyl nodes by solving the quantum Boltzmann equation (QBE). The RG analysis above is performed for the massless Dirac fermions with N species. One massless Dirac fermion can be separated into two Weyl fermions with opposite chiralities, therefore N Dirac nodes can be interpreted as $2N$ Weyl nodes, and we put $N_{\mathrm{W}} = 2N$.

1. The Quantum Boltzmann equation

The QBE is the matrix equation, whose elements are labeled by fermion species, spin, and helicity indices. We focus on the right-handed electron with species a, and there are N copies of right-handed electrons and a corresponding number of left-handed particles.

Calculations are done by following previous studies.[13,18,19] We only focus on the diagonal elements of the QBE, which describe the distribution functions of particles and holes $f_{\lambda a}(\boldsymbol{k}, t)$. Here, $\lambda = \pm$ represents a particle ($\lambda = +$) or a hole ($\lambda = -$), and a denotes a Weyl fermion species. The off-diagonal elements correspond to the particle-hole pair contribution, and for $\omega \ll T$, its contribution is suppressed.[13] Then, the QBE in the external field $\boldsymbol{F}$ is

$$\left[\frac{\partial}{\partial t} + \boldsymbol{F} \cdot \frac{\partial}{\partial \boldsymbol{k}}\right] f_{\lambda a}(\boldsymbol{k}, t) = -w[f_{\lambda a}(\boldsymbol{k}, t)], \tag{A.1}$$

where the scattering rate w reflects the electron correlation effect. The scattering rate $w[f_{\lambda a}(\boldsymbol{k}, t)]$ is written as

$$\begin{aligned} w[f_{\lambda a}(\boldsymbol{k}, t)] = \frac{1}{2} \sum_{\substack{bcd \\ \lambda_1 \lambda_2 \lambda_3}} \int_{\boldsymbol{p}, \boldsymbol{k}', \boldsymbol{p}'} & \left| M^{\lambda a, \lambda_1 b}_{\lambda_2 c, \lambda_3 d}(k, p, k', p') \right|^2 \\ & \times (2\pi) \delta(E_{\lambda a}(k) + E_{\lambda_1 b}(p) - E_{\lambda_2 c}(k') - E_{\lambda_3 d}(p')) \\ & \times (2\pi)^3 \delta^{(3)}(\boldsymbol{k} + \boldsymbol{p} - \boldsymbol{k}' - \boldsymbol{p}') \\ & \times \big\{ f_{\lambda a}(\boldsymbol{k}, t) f_{\lambda_1 b}(\boldsymbol{p}, t) [1 - f_{\lambda_2 c}(\boldsymbol{k}', t)][1 - f_{\lambda_3 d}(\boldsymbol{p}', t)] \\ & - [1 - f_{\lambda a}(\boldsymbol{k}, t)][1 - f_{\lambda_1 b}(\boldsymbol{p}, t)] f_{\lambda_2 c}(\boldsymbol{k}', t) f_{\lambda_3 d}(\boldsymbol{p}', t) \big\}. \end{aligned} \tag{A.2}$$

Here, $E_{\lambda a}(k) = \lambda v k$ is the energy of the ath Weyl node. We only consider the two-body scattering, and $M^{\lambda a, \lambda_1 b}_{\lambda_2 c, \lambda_3 d}(k, p, k', p')$ is the scattering amplitude with nonrelativistic renormalization. The relation to the relativistic scattering amplitude $\mathcal{M}$ is

$$\left| M^{\lambda a, \lambda_1 b}_{\lambda_2 c, \lambda_3 d}(k, p, k', p') \right|^2 = \frac{\left| \mathcal{M}^{\lambda a, \lambda_1 b}_{\lambda_2 c, \lambda_3 d}(k, p, k', p') \right|^2}{(2E_{\lambda a})(2E_{\lambda_1 b})(2E_{\lambda_2 c})(2E_{\lambda_3 d})}. \tag{A.3}$$

We assume that the external electric force $\boldsymbol{F} = e\boldsymbol{E}$ is weak, and that the deviation of the distribution function from the equilibrium $f^0_{\lambda a}(k) = (1 + e^{\beta E_{\lambda a}(k)})^{-1}$ is small, so that we consider the linear response in $\boldsymbol{E}$:

$$f_{\lambda a}(\boldsymbol{k}, \omega) = 2\pi \delta(\omega) f^0_{\lambda a}(k) + \lambda \frac{\boldsymbol{k} \cdot e\boldsymbol{E}(\omega)}{k} f^0_{\lambda a}(k)[1 - f^0_{\lambda a}(k)] g_a(k, \omega). \tag{A.4}$$

The current density $\boldsymbol{j}(\omega)$, without the particle-hole pair contribution, is

$$\boldsymbol{j}(\omega) = ev \sum_{\lambda a} \int_{\boldsymbol{k}} \frac{\lambda \boldsymbol{k}}{k} f_{\lambda a}(\boldsymbol{k}, \omega), \tag{A.5}$$

therefore, the electric conductivity $\sigma(\omega)$ is given by using the function $g(k, \omega)$ as

$$\sigma(\omega) = \frac{j(\omega)}{E(\omega)} = e^2 v \sum_{\lambda a} \int_{\boldsymbol{k}} \frac{k_x^2}{k^2} f^0_{\lambda a}(k)[1 - f^0_{\lambda a}(k)] g_a(k, \omega). \tag{A.6}$$

We should determine $g(k,\omega)$ to obtain the electric conductivity. In equilibrium, the scattering rate vanishes, i.e., $w[f^0]=0$, so when we expand the scattering rate in terms of $g(k,\omega)$, the zeroth order term vanishes, and we can write

$$w[f_{\lambda a}(\boldsymbol{k},\omega)] = e\boldsymbol{E}(\omega)\cdot\mathcal{C}[\lambda g(k,\omega)\hat{\boldsymbol{k}}] + O(g^2), \tag{A.7}$$

where $\hat{\boldsymbol{k}}=\boldsymbol{k}/k$, and $\mathcal{C}$ is called the collision operator. The collision operator is given by

$$\begin{aligned}
&\mathcal{C}[\lambda\hat{\boldsymbol{k}}g_a(k,\omega)]\\
&=\frac{1}{2}\sum_{\substack{bcd\\ \lambda_1\lambda_2\lambda_3}}\int_{\boldsymbol{p},\boldsymbol{k}',\boldsymbol{p}'}\left|M^{\lambda a,\lambda_1 b}_{\lambda_2 c,\lambda_3 d}(k,p,k',p')\right|^2\\
&\qquad\qquad\times(2\pi)\delta(E_{\lambda a}(k)+E_{\lambda_1 b}(p)-E_{\lambda_2 c}(k')+E_{\lambda_3 d}(p'))\\
&\qquad\qquad\times(2\pi)^3\delta^{(3)}(\boldsymbol{k}+\boldsymbol{p}-\boldsymbol{k}'-\boldsymbol{p}')\\
&\qquad\qquad\times f^0_{\lambda a}(k)f^0_{\lambda_1 b}(p)[1-f^0_{\lambda_2 c}(k')][1-f^0_{\lambda_3 d}(p')]\\
&\qquad\qquad\times\left[\lambda\hat{\boldsymbol{k}}g_a(k,\omega)+\lambda_1\hat{\boldsymbol{p}}g_b(p,\omega)-\lambda_2\hat{\boldsymbol{k}}'g_c(k',\omega)-\lambda_3\hat{\boldsymbol{p}}'g_d(p',\omega)\right].
\end{aligned}\tag{A.8}$$

By using the collision operator, the QBE becomes

$$[i\omega g_a(k,\omega)+\beta v]\,\lambda\hat{\boldsymbol{k}}f^0_{\lambda a}(k)[1-f^0_{\lambda a}(k)] = \mathcal{C}[\lambda\hat{\boldsymbol{k}}g_a(k,\omega)]. \tag{A.9}$$

To solve this equation, it it convenient to use a variational method. The variational functional $\mathcal{Q}[g]$ is derived by defining the inner product. We define the inner product as

$$\langle F,G\rangle = \sum_a\int_{\boldsymbol{k}} F_a(\boldsymbol{k})\cdot G_a(\boldsymbol{k}), \tag{A.10}$$

and the functional $\mathcal{Q}[g]$ is given by

$$\mathcal{Q}[g] = \sum_a\int_{\boldsymbol{k}}\left[i\omega\frac{g_a^2(k,\omega)}{2}+\beta v g_a(k,\omega)\right]f^0_{\lambda a}(k)[1-f^0_{\lambda a}(k)] - \frac{1}{2}\langle\lambda\hat{\boldsymbol{k}}g_a(k,\omega),\mathcal{C}[\lambda\hat{\boldsymbol{k}}g_a(k,\omega)]\rangle. \tag{A.11}$$

The product $\langle\lambda\hat{\boldsymbol{k}}g_a,\mathcal{C}[\lambda\hat{\boldsymbol{k}}g_a]\rangle$ is expressed as

$$\begin{aligned}
&\langle\lambda\hat{\boldsymbol{k}}g_a,\mathcal{C}[\lambda\hat{\boldsymbol{k}}g_a]\rangle\\
&=\frac{1}{8}\sum_{\substack{abcd\\ \lambda_1\lambda_2\lambda_3}}\int_{\boldsymbol{k},\boldsymbol{p},\boldsymbol{q}}\left|M^{\lambda a,\lambda_1 b}_{\lambda_2 c,\lambda_3 d}\right|^2(2\pi)\delta(E_{\lambda a}(k)+E_{\lambda_1 b}(p)-E_{\lambda_2 c}(k')+E_{\lambda_3 d}(p'))\\
&\qquad\times f^0_{\lambda a}(k)f^0_{\lambda_1 b}(p)[1-f^0_{\lambda_2 c}(|\boldsymbol{k}+\boldsymbol{q}|)][1-f^0_{\lambda_3 d}(|\boldsymbol{p}-\boldsymbol{q}|)]\\
&\qquad\times\left[\lambda\frac{\boldsymbol{k}}{|\boldsymbol{k}|}g_a(k,\omega)+\lambda_1\frac{\boldsymbol{p}}{|\boldsymbol{p}|}g_b(p,\omega)-\lambda_2\frac{\boldsymbol{k}+\boldsymbol{q}}{|\boldsymbol{k}+\boldsymbol{q}|}g_c(|\boldsymbol{k}+\boldsymbol{q}|,\omega)-\lambda_3\frac{\boldsymbol{p}-\boldsymbol{q}}{|\boldsymbol{p}-\boldsymbol{q}|}g_d(|\boldsymbol{p}-\boldsymbol{q}|,\omega)\right]^2,
\end{aligned}\tag{A.12}$$

where $\boldsymbol{q}=\boldsymbol{k}'-\boldsymbol{k}$ comes from the momentum conservation. In this calculation, we assume that all Weyl nodes are equivalent, so $f^0_{\lambda a}(k)$ and $g_a(k,\omega)$ is independent of the species. Thus, we omit the index a and use $f^0_\lambda(k)$ and $g(k,\omega)$ in the following calculation. The stationary point

$$\frac{\delta\mathcal{Q}[g]}{\delta g}=0 \tag{A.13}$$

gives the solution $g(k,\omega)$.

2. Scattering rate

The next task is to calculate the functional $\langle\lambda\hat{\boldsymbol{k}}g_a,\mathcal{C}[\lambda\hat{\boldsymbol{k}}g_a]\rangle$. For simplicity, we set $\lambda=+$ and $a=\mathrm{R}$, where the handedness of the species is represented as $a=\mathrm{R}$ or L. There are four scattering processes we should consider (Fig. 7).

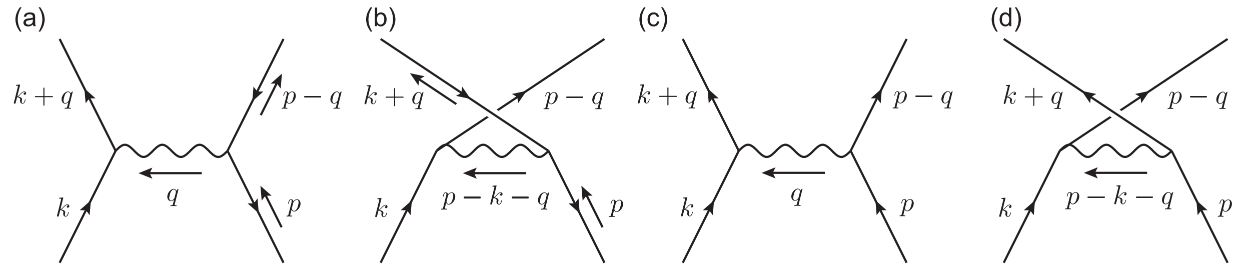

FIG. 7. Feynman diagrams for the leading order two-particle scattering processes. (a) and (b) represent electron-hole scatterings, and (c) and (d) electron-electron scatterings. The t-channel diagrams [(a) and (c)] contribute to the leading order in the LLA, while the u-channel diagrams [(b) and (d)] do not.

We write the scattering rate of electron-hole and electron-election process as $R_1(\boldsymbol{k},\boldsymbol{p},\boldsymbol{q})$ and $R_2(\boldsymbol{k},\boldsymbol{p},\boldsymbol{q})$, respectively, where $\boldsymbol{q}$ is the momentum of the virtual photon. Then, the functional $\langle\hat{\boldsymbol{k}}g,\mathcal{C}[\hat{\boldsymbol{k}}g]\rangle$ becomes

$$\begin{aligned}
&\langle\hat{\boldsymbol{k}}g,\mathcal{C}[\hat{\boldsymbol{k}}g]\rangle \\
&=\frac{1}{8}\int_{\boldsymbol{k},\boldsymbol{p},\boldsymbol{q}}\frac{2\pi}{v}\Bigg\{\delta(k-p-|\boldsymbol{k}+\boldsymbol{q}|+|\boldsymbol{p}-\boldsymbol{q}|) \\
&\qquad\times f_+^0(k)f_-^0(p)[1-f_+^0(|\boldsymbol{k}+\boldsymbol{q}|)][1-f_-^0(|\boldsymbol{p}-\boldsymbol{q}|)]R_1(\boldsymbol{k},\boldsymbol{p},\boldsymbol{q}) \\
&\qquad\times\left[\frac{\boldsymbol{k}}{|\boldsymbol{k}|}g(k,\omega)-\frac{\boldsymbol{p}}{|\boldsymbol{p}|}g(p,\omega)-\frac{\boldsymbol{k}+\boldsymbol{q}}{|\boldsymbol{k}+\boldsymbol{q}|}g(|\boldsymbol{k}+\boldsymbol{q}|,\omega)+\frac{\boldsymbol{p}-\boldsymbol{q}}{|\boldsymbol{p}-\boldsymbol{q}|}g(|\boldsymbol{p}-\boldsymbol{q}|,\omega)\right]^2 \\
&\quad+\delta(k+p-|\boldsymbol{k}+\boldsymbol{q}|-|\boldsymbol{p}-\boldsymbol{q}|) \\
&\qquad\times f_+^0(k)f_+^0(p)[1-f_+^0(|\boldsymbol{k}+\boldsymbol{q}|)][1-f_+^0(|\boldsymbol{p}-\boldsymbol{q}|)]R_2(\boldsymbol{k},\boldsymbol{p},\boldsymbol{q}) \\
&\qquad\times\left[\frac{\boldsymbol{k}}{|\boldsymbol{k}|}g(k,\omega)+\frac{\boldsymbol{p}}{|\boldsymbol{p}|}g(p,\omega)-\frac{\boldsymbol{k}+\boldsymbol{q}}{|\boldsymbol{k}+\boldsymbol{q}|}g(|\boldsymbol{k}+\boldsymbol{q}|,\omega)-\frac{\boldsymbol{p}-\boldsymbol{q}}{|\boldsymbol{p}-\boldsymbol{q}|}g(|\boldsymbol{p}-\boldsymbol{q}|,\omega)\right]^2\Bigg\},
\end{aligned}\tag{A.14}$$

and the scattering rate is

$$\begin{aligned}
R_1(\boldsymbol{k},\boldsymbol{p},\boldsymbol{q})&=|M^{+\mathrm{R},-\mathrm{R}}_{+\mathrm{R},-\mathrm{R}}(\boldsymbol{k},\boldsymbol{p},\boldsymbol{q})-M^{+\mathrm{R},-\mathrm{R}}_{-\mathrm{R},+\mathrm{R}}(\boldsymbol{k},\boldsymbol{p},\boldsymbol{p}-\boldsymbol{k}-\boldsymbol{q})|^2 \\
&\quad+(N-1)\left[|M^{+\mathrm{R},-\mathrm{R}}_{+\mathrm{R},-\mathrm{R}}(\boldsymbol{k},\boldsymbol{p},\boldsymbol{q})|^2+|M^{+\mathrm{R},-\mathrm{R}}_{-\mathrm{R},+\mathrm{R}}(\boldsymbol{k},\boldsymbol{p},\boldsymbol{p}-\boldsymbol{k}-\boldsymbol{q})|^2\right] \\
&\quad+N\left[|M^{+\mathrm{R},-\mathrm{L}}_{+\mathrm{R},-\mathrm{L}}(\boldsymbol{k},\boldsymbol{p},\boldsymbol{q})|^2+|M^{+\mathrm{R},-\mathrm{L}}_{-\mathrm{L},+\mathrm{R}}(\boldsymbol{k},\boldsymbol{p},\boldsymbol{p}-\boldsymbol{k}-\boldsymbol{q})|^2\right] \\
R_2(\boldsymbol{k},\boldsymbol{p},\boldsymbol{q})&=\frac{1}{2}|M^{+\mathrm{R},+\mathrm{R}}_{+\mathrm{R},+\mathrm{R}}(\boldsymbol{k},\boldsymbol{p},\boldsymbol{q})-M^{+\mathrm{R},+\mathrm{R}}_{+\mathrm{R},+\mathrm{R}}(\boldsymbol{k},\boldsymbol{p},\boldsymbol{p}-\boldsymbol{k}-\boldsymbol{q})|^2 \\
&\quad+(N-1)|M^{+\mathrm{R},+\mathrm{R}}_{+\mathrm{R},+\mathrm{R}}(\boldsymbol{k},\boldsymbol{p},\boldsymbol{q})|^2+N|M^{+\mathrm{R},+\mathrm{L}}_{+\mathrm{R},+\mathrm{L}}(\boldsymbol{k},\boldsymbol{p},\boldsymbol{q})|^2.
\end{aligned}\tag{A.15}$$

We assume the form $g(k,\omega)=k\xi(\omega)$ according to Fritz *et al.*[19] In this case, only the electron-hole scatterings [Fig. 7 (a), (b)] contribute, and the electron-electron scatterings [Fig. 7 (c), (d)] do not.

In the leading log approximation (LLA), the divergence at small q plays a key role. In other words, the integrand proportional to $1/q$ gives a logarithmic divergence, and this is the dominant contribution in the LLA. As we can see from the Feynman diagrams, only the t-channel diagrams [Fig. 7 (a), (c)], in which the photon propagators give $1/q^2$ contribution, are proportional to $1/q$, and must be retained. The u-channel diagrams [Fig. 7 (b), (d)] give finite contributions, and they can be ignored in the LLA.

Therefore, only the contribution from Fig. 7 (a) should be retained, and it is necessary to calculate

$$R_1(\boldsymbol{k},\boldsymbol{p},\boldsymbol{q})\sim N|M^{+\mathrm{R},-\mathrm{R}}_{+\mathrm{R},-\mathrm{R}}(\boldsymbol{k},\boldsymbol{p},\boldsymbol{q})|^2+N|M^{+\mathrm{R},-\mathrm{L}}_{+\mathrm{R},-\mathrm{L}}(\boldsymbol{k},\boldsymbol{p},\boldsymbol{q})|^2.\tag{A.16}$$

For a later use, we write the delta function originated from the energy conservation as

$$\delta(k-p-|\boldsymbol{k}+\boldsymbol{q}|+|\boldsymbol{p}-\boldsymbol{q}|)=\int_{-\infty}^{\infty}\delta(k-|\boldsymbol{k}+\boldsymbol{q}|+\Omega)\delta(p-|\boldsymbol{p}-\boldsymbol{q}|+\Omega)d\Omega.\tag{A.17}$$

By using the projection operator $(1 \pm \gamma^5)/2$, we can calculate the relativistic scattering rate $|\mathcal{M}^{+\mathrm{R},-\mathrm{R}}_{+\mathrm{R},-\mathrm{R}}(k,p,k',p')|^2$ and $|\mathcal{M}^{+\mathrm{R},-\mathrm{L}}_{+\mathrm{R},-\mathrm{L}}(k,p,k',p')|^2$. After some calculations and taking spin sums, the scattering rates become

$$\begin{aligned}
&\sum_{\text{spins}} |\mathcal{M}^{+\mathrm{R},-\mathrm{R}}_{+\mathrm{R},-\mathrm{R}}(k,p,k',p')|^2 \\
=&\frac{8e^4c^4}{\varepsilon q_\mathrm{p}^4}\Bigg\{(lk_\mathrm{e}\cdot lp_\mathrm{e})(lk'_\mathrm{e}\cdot lp'_\mathrm{e}) + (lk_\mathrm{e}\cdot lp'_\mathrm{e})(lk'_\mathrm{e}\cdot lp_\mathrm{e}) - (l^2k_\mathrm{e}\cdot l^2k'_\mathrm{e})(p_\mathrm{e}\cdot p'_\mathrm{e}) - (k_\mathrm{e}\cdot k'_\mathrm{e})(l^2p_\mathrm{e}\cdot l^2p'_\mathrm{e}) \\
&\quad + \frac{1}{2}\left[1+3\left(\frac{v}{c}\right)\right](k_\mathrm{e}\cdot k'_\mathrm{e})(p_\mathrm{e}\cdot p'_\mathrm{e}) + \left(\frac{v}{c}\right)^6\left[(k_\mathrm{p}\cdot p'_\mathrm{p})(k'_\mathrm{p}\cdot p_\mathrm{e}) - (k_\mathrm{p}\cdot p_\mathrm{p})(k'_\mathrm{p}\cdot p'_\mathrm{p})\right]\Bigg\},
\end{aligned} \tag{A.18}$$

$$\begin{aligned}
&\sum_{\text{spins}} |\mathcal{M}^{+\mathrm{R},-\mathrm{L}}_{+\mathrm{R},-\mathrm{L}}(k,p,k',p')|^2 \\
=&\frac{8e^4c^4}{\varepsilon q_\mathrm{p}^4}\Bigg\{(lk_\mathrm{e}\cdot lp_\mathrm{e})(lk'_\mathrm{e}\cdot lp'_\mathrm{e}) + (lk_\mathrm{e}\cdot lp'_\mathrm{e})(lk'_\mathrm{e}\cdot lp_\mathrm{e}) - (l^2k_\mathrm{e}\cdot l^2k'_\mathrm{e})(p_\mathrm{e}\cdot p'_\mathrm{e}) - (k_\mathrm{e}\cdot k'_\mathrm{e})(l^2p_\mathrm{e}\cdot l^2p'_\mathrm{e}) \\
&\quad + \frac{1}{2}\left[1+3\left(\frac{v}{c}\right)\right](k_\mathrm{e}\cdot k'_\mathrm{e})(p_\mathrm{e}\cdot p'_\mathrm{e}) - \left(\frac{v}{c}\right)^6\left[(k_\mathrm{p}\cdot p'_\mathrm{p})(k'_\mathrm{p}\cdot p_\mathrm{e}) - (k_\mathrm{p}\cdot p_\mathrm{p})(k'_\mathrm{p}\cdot p'_\mathrm{p})\right]\Bigg\},
\end{aligned} \tag{A.19}$$

where $k_\mathrm{e} = (k, v\boldsymbol{k})$ is an electron four-vector and $k_\mathrm{p} = (k, c\boldsymbol{k})$ is a photon four-vector. We set the spherical coordinates with $\boldsymbol{q}$ as the z axis and choose the x axis so that $\boldsymbol{p}$ lies in the zx plane. ϕ is the the azimuthal angle of $\boldsymbol{k}$. In the LLA, the scattering rates can be simplified as

$$\begin{aligned}
&\int_0^{2\pi} d\phi \sum_{\text{spins}} |\mathcal{M}^{+\mathrm{R},-\mathrm{R}}_{+\mathrm{R},-\mathrm{R}}(k,p,k',p')|^2 \simeq \int_0^{2\pi} d\phi \sum_{\text{spins}} |\mathcal{M}^{+\mathrm{R},-\mathrm{L}}_{+\mathrm{R},-\mathrm{L}}(k,p,k',p')|^2 \\
\simeq&\frac{16e^4}{\varepsilon^2}(2\pi)v^4\frac{(pk)^2}{q^4}\left[1+\frac{1}{2}\left(\frac{v}{c}\right)^4\left(\frac{q^2-\Omega^2}{q^2-\left(\frac{v}{c}\right)^2\Omega^2}\right)^2\right].
\end{aligned} \tag{A.20}$$

As we stated before, the integral over q is logarithmically divergent, so we need to introduce the upper and lower cutoffs. Here, we assume that the momentum q is small, and this approximation is valid for $q \lesssim T/v$. So the upper cutoff should be T/v. The lower cutoff is emerged from the absence of a thermal self-energy insertion. This divergence will be removed by introducing higher-order perturbative corrections to the fermion self-energy, and such corrections appear at order α correction. Thus, the fermion propagator without self-energy insertion is invalid for $q \lesssim \alpha T/v$, and the lower cutoff should be $\alpha T/v$. Then, the integral over q bocomes

$$\int_0^\infty \frac{dq}{q} \simeq \int_{\alpha T/v}^{T/v} \frac{dq}{q} = \ln \alpha^{-1}. \tag{A.21}$$

After complicated but straight-forward calculations, we finally obtain the functional $\langle \hat{\boldsymbol{k}}g, \mathcal{C}[\hat{\boldsymbol{k}}g]\rangle$ as

$$\langle \hat{\boldsymbol{k}}g, \mathcal{C}[\hat{\boldsymbol{k}}g]\rangle = \frac{\pi N_\mathrm{W}}{9\beta^6 v^5}(\alpha^2 \ln \alpha^{-1}) F\left(\frac{v}{c}\right)[\xi(\omega)]^2, \tag{A.22}$$

and the variational functional $\mathcal{Q}[k\xi(\omega)]$ is

$$\begin{aligned}
\mathcal{Q}[k\xi(\omega)] = &\frac{1}{4\pi^2}\frac{1}{(\beta v)^5}\left\{i\omega\frac{7\pi^4}{30}[\xi(\omega)]^2 + 9(\beta v)^2\zeta(3)\xi(\omega)\right\} \\
&- \frac{1}{2}\frac{\pi N_\mathrm{W}}{9\beta^6 v^5}(\alpha^2 \ln \alpha^{-1}) F\left(\frac{v}{c}\right)[\xi(\omega)]^2,
\end{aligned} \tag{A.23}$$

with the relativistic correction $F(v/c)$ [eq. (64)].

3. Solution

Now that we have the variational functional $\mathcal{Q}[k\xi(\omega)]$, we can determine $\xi(\omega)$ by the functional derivative as

$$\xi(\omega) = \frac{81\zeta(3)}{4\pi^3}\beta^3 v^2\left[N_\mathrm{W}(\alpha^2 \ln \alpha^{-1}) F\left(\frac{v}{c}\right) - \frac{21\pi}{20} i\beta\omega\right]^{-1}. \tag{A.24}$$

Then, the electric conductivity in the LLA is

$$\begin{aligned}\sigma^{(N)}(\omega,T) =& e^2 v \sum_{\lambda a}\int_{\boldsymbol{k}} \frac{k_x^2}{k^2}\frac{1}{\beta v}\left(-\frac{\partial f_\lambda^0(k)}{\partial k}\right) k\xi(\omega)\\ =&\frac{3\zeta(3)}{2\pi^2}N_{\mathrm{W}}\frac{e^2}{\beta^4 v^3}\xi(\omega)\\ =&N_{\mathrm{W}}\frac{e^2}{h^2}\left(\frac{k_{\mathrm{B}}T}{\hbar v}\right)\frac{243[\zeta(3)]^2}{4\pi^4}\left[N_{\mathrm{W}}(\alpha^2\ln\alpha^{-1})F\left(\frac{v}{c}\right)-\frac{21\pi}{20}i\beta\omega\right]^{-1}. \end{aligned} \tag{A.25}$$

We recovered k_{B} and $\hbar$ in the last line of the equation.

---

[1] For a description of the Dirac equation and QED, see for example M. E. Peskin and D. V. Schroeder, *An Introduction to Quantum Field Theory* (Westview Press, 1995); P. Ramond, *Field Theory: A Modern Primer*, 2nd ed. (Addison-Wesley, 1990).

[2] H. Nielsen and M. Ninomiya, Phys. Lett. B **130**, 389 (1983).

[3] A. H. Castro Neto, F. Guinea, N. M. R. Peres, K. S. Novoselov, and A. K. Geim, Rev. Mod. Phys. **81**, 109 (2009).

[4] Y. Fuseya, M. Ogata, and H. Fukuyama, Phys. Rev. Lett. **102**, 066601 (2009) and references therein.

[5] M. Z. Hasan and C. L. Kane, Rev. Mod. Phys. **82**, 3045 (2010).

[6] X.-L. Qi and S.-C. Zhang, Rev. Mod. Phys. **83**, 1057 (2011).

[7] S.-Y. Xu, Y. Xia, L. A. Wray, S. Jia, F. Meier, J. H. Dil, J. Osterwalder, B. Slomski, A. Bansil, H. Lin, R. J. Cava, and M. Z. Hasan, Science **332**, 560 (2011).

[8] T. Sato, K. Segawa, K. Kosaka, S. Souma, K. Nakayama, K. Eto, T. Minami, Y. Ando, and T. Takahashi, Nature Phys. **7**, 840 (2011).

[9] X. Wan, A. M. Turner, A. Vishwanath, and S. Y. Savrasov, Phys. Rev. B **83**, 205101 (2011).

[10] W. Witczak-Krempa and Y. B. Kim, Phys. Rev. B **85**, 045124 (2012).

[11] V. N. Kotov, B. Uchoa, V. M. Pereira, F. Guinea, and A. H. Castro Neto, Rev. Mod. Phys. **84**, 1067 (2012).

[12] P. Goswami and S. Chakravarty, Phys. Rev. Lett. **107**, 196803 (2011).

[13] P. Hosur, S. A. Parameswaran, and A. Vishwanath, Phys. Rev. Lett. **108**, 046602 (2012).

[14] J. González, F. Guinea, and M. Vozmediano, Nucl. Phys. B **424**, 595 (1994).

[15] H. Isobe and N. Nagaosa, Phys. Rev. B **86**, 165127 (2012).

[16] G. S. Adkins, Phys. Rev. D **27**, 1814 (1983).

[17] For example, we calculate the electron velocity v in Coulomb gauge. Its bare value is obtained by $v_{\mathrm{B}} = vZ_{2\mathrm{s}}^{(\mathrm{C})}/Z_{2\mathrm{t}}^{(\mathrm{C})}$. We can see that this equation is exactly the same as the result in Feynman gauge. Thus, the running electron velocity $v(\kappa)$ is unchanged whichever gauge we choose.

[18] P. Arnold, G. D. Moore, and L. G. Yaffe, J. High Energy Phys. **11**, 001 (2000).

[19] L. Fritz, J. Schmalian, M. Müller, and S. Sachdev, Phys. Rev. B **78**, 085416 (2008).

[20] X.-L. Qi, R. Li, J. Zang, and S.-C. Zhang, Science **323**, 1184 (2009).